



# HHS Public Access

Author manuscript

*Chem Res Toxicol.* Author manuscript; available in PMC 2019 July 29.

Published in final edited form as:

*Chem Res Toxicol.* 2019 January 22; 32(1): 113–121. doi:10.1021/acs.chemrestox.8b00218.

## Lateral Flow Assessment and Unanticipated Toxicity of Kratom

Lauren C. Smith<sup>†</sup>, Lucy Lin<sup>†</sup>, Candy S. Hwang<sup>†,||</sup>, Bin Zhou<sup>†</sup>, Diane M. Kubitz<sup>‡</sup>, Huiying Wang<sup>§</sup>, Kim D. Janda<sup>\*,†</sup>

<sup>†</sup>Departments of Chemistry, Immunology and Microbial Science, Skaggs Institute for Chemical Biology

<sup>‡</sup>Center for Antibody Development and Production; The Scripps Research Institute, La Jolla, California 92037 United States

<sup>§</sup>ABiox Company, 720 East First Street, Newberg, Oregon 97132, United States

### Abstract

The leaves of the *Mitragynine speciosa* tree (also known as Kratom) have long been chewed, smoked, or brewed into a tea by people in Southeastern Asian countries, such as Malaysia and Thailand. Just this past year, the plant Kratom gained popularity in the United States as a “legal opioid” and scheduling it as a drug of abuse is currently pending. The primary alkaloid found in Kratom is a  $\mu$ -opioid receptor agonist, mitragynine, whose structure contains a promising scaffold for immunopharmacological use. Although Kratom is regarded as a safe opioid alternative, here we report the LD<sub>50</sub> values determined for its two main psychoactive alkaloids, mitragynine and 7-hydroxymitragynine, as comparable to heroin in mice when administered intravenously. Given Kratom’s recent emergence in the U.S., there is currently no diagnostic test available for law enforcement or health professionals, so we sought to design such an assay. Mitragynine was used as a starting point for hapten design, resulting in a hapten with an ether linker extending from the C9 position of the alkaloid. Bacterial flagellin (FliC) was chosen as a carrier protein for active immunization in mice, yielding 32 potential monoclonal antibodies (mAbs) for assay development. Antimitragynine mAbs in the range of micro- to nanomolar affinities were uncovered and their utility in producing a convenient lateral flow detection assay of human fluid samples was examined. Antibodies were screened for binding to mitragynine, 7-hydroxymitragynine, and performance in lateral flow assays. Two monoclonal antibodies were subcloned and further purified with 93 and 362 nM affinity to mitragynine. Test strip assays were

\*Corresponding Author kdjanda@scripps.edu.

<sup>||</sup> Present Address Department of Chemistry, Southern Connecticut State University, 501 Crescent St., New Haven, CT 06515, USA.

Author Contributions  
All authors have given approval to the final version of the manuscript. Manuscript was written by L.C.S. and edited by C.S.H. and K.D.J. All artwork for figures and TOC graphic was created by L.C.S.. Lethality experiments were performed by L.C.S. and C.S.H. Hapten synthesis was completed by L.C.S. and L.L. Immunoconjugation and vaccine preparation was performed by L.C.S. Mouse immunization and monoclonal antibody production was performed by D.M.K. SPR screening and final kinetics data were completed by B.Z. Competitive ELISA screening was executed by L.C.S. Lateral flow assay development was completed by L.C.S. with technical advice from H.W.

#### ASSOCIATED CONTENT

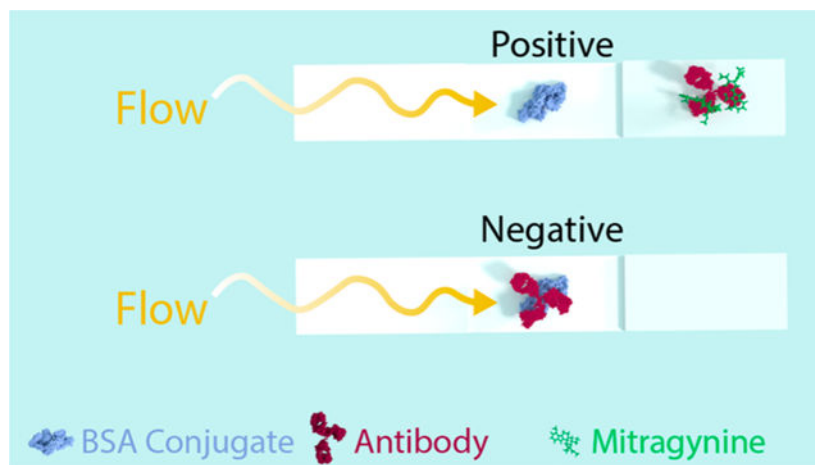
##### Supporting Information

The Supporting Information is available free of charge on the ACS Publications website at DOI: [10.1021/acs.chemrestox.8b00218](https://doi.org/10.1021/acs.chemrestox.8b00218). Detailed data include hapten characterization by NMR and HPLC, immunoconjugate characterization by MALDI-ToF spectra, lethality curves, 32-hybridoma panel midpoint titers and SPR, and competitive ELISA curves and IC<sub>50</sub>'s for all mAbs run (PDF)

The authors declare no competing financial interest.

optimized with a detection cut off of 0.5  $\mu\text{g}/\text{mL}$  for mitragynine in buffer and urine (reflecting projected clinically relevant levels of drug in urine), which could be beneficial to law enforcement agencies and health professionals as the opioid epidemic in America continues to evolve.

## Graphical Abstract



## INTRODUCTION

In the wake of an ever-growing opioid epidemic, the scientific community is searching for a “cure” for substance abuse disorders. *Mitragyna speciosa*, also referred to as Kratom, in the Rubiaceae family has been used for centuries as a “natural” pain-relieving herbal supplement in Southeastern Asia.<sup>1</sup> The two most active alkaloids in Kratom are the opioid analgesics, mitragynine and 7-hydroxymitragynine (Figure 1). Of these two, mitragynine is the most abundant, consisting of about 66% of the plant’s extract, while 7-hydroxymitragynine only constitutes about 2%.<sup>2</sup> Although several countries, namely Thailand and Malaysia, have endured the plant’s widespread abuse, Kratom is only now penetrating the U.S. market.<sup>3</sup> Kratom-induced overdose is thought to be rare and usually caused by a stronger opioid contaminant.<sup>4,5</sup> However, this is a grave misconception.

In February of 2018, the FDA released a statement reporting 44 cases of Kratom-related overdose deaths in U.S. within the past few years.<sup>6</sup> Kratom has recently garnered additional negative media attention due to several *Salmonella* outbreaks across the U.S.<sup>7</sup> Abuse of this unregulated drug in America will likely increase in the years to come, whereas research on its main alkaloids, their safety, mechanism of action(s), and detection methods remain relatively unexplored.

The opioid receptors, classified as  $\mu$ -,  $\kappa$ -, and  $\delta$ -, belong to a large transmembrane superfamily of G-protein coupled receptors. Opioid ligand binding to these receptors trigger binding to the G-protein and formation of a GTP complex, which is responsible for inhibition of adenylyl cyclase and reduction of cAMP levels. This intracellular pathway affects changes in membrane currents and causes inhibition of transmitter release, leading to biological responses such as analgesia and euphoria.<sup>8</sup> Agonists at the  $\mu$ -opioid receptors

(OR) commonly produce the undesired side effects of respiratory depression, constipation, vomiting, and nausea due to the presence of  $\mu$ -OR on neurons at respiratory control centers in the pons and brainstem, as well as in the gastrointestinal tract.<sup>9</sup> Several studies have shown that the mitragynine family of alkaloids is unique to the opioid drug class in that they have a G-protein response bias over  $\beta$ -arrestin.<sup>10–12</sup> This ligand bias is an attractive moving target for medicinal chemists in the search for an opioid analgesic that does not induce the undesired side effects at the  $\mu$ -OR. In 2016, Kruegel et al. reported mitragynine bound to the murine  $\mu$ -OR as a competitive antagonist.<sup>13</sup> This observation conflicts with previous reports that the antinociceptive effects of mitragynine and  $\mu$ -hydroxymitragynine are inhibited by naloxone, a confirmed  $\mu$ -OR competitive antagonist, in several rodent models.<sup>10,11,14</sup>

To date, there has only been one report demonstrating the production of monoclonal antibodies (mAbs) against mitragynine, with binding affinities in the millimolar range.<sup>15</sup> Although this antibody was developed into an ELISA and a lateral flow assay, the detection limits are in the mg/mL range.<sup>16</sup> Otherwise, detection of mitragynine and its metabolites at the nanomolar level requires high-pressure liquid chromatography (HPLC) and tandem liquid chromatography mass spectrometry (LC/MS) instruments. Lateral flow assays are the ideal technology for drug detection in biological samples due to their cost, efficiency, and portability.

Kratom's rise in popularity has caused the need for an easy and reliable detection method, such as lateral flow immuno-assay for analyzing human fluid samples. This study was designed and carried out in three phases. First phase was the design and synthesis of a mitragynine hapten, its subsequent immunoconjugation, and vaccine formulation (Figure 2A). The second phase was monoclonal antibody production in mice after active vaccination (Figure 2B), followed by the third phase of lateral flow strip design, production, and optimization (Figure 2C).

## EXPERIMENTAL PROCEDURES

### Methyl (*E*)-2-((2*S*,3*S*)-3-ethyl-8-hydroxy-1,2,3,4,6,7,12,12*b*-octahydromdolo[2,3-*a*]quinoxalin-2-yl)-3-methoxyacrylate (**2**).<sup>11,13</sup>

A solution of mitragynine (0.2 g, 0.5 mmol) in dry DCM (2.7 mL) was added dropwise to a stirred solution of  $\text{AlCl}_3$  (0.2 g, 1.5 mmol) (Figures S1,2) in ethanethiol (0.7 mL, 9 mmol) at 0 °C under argon atmosphere and stirred for 3 h at room temperature (rt). The reaction was quenched with water, neutralized with dilute HCl, and extracted three times with DCM. The combined extracts were washed with brine, dried over  $\text{MgSO}_4$ , and evaporated to give 0.192 mg (99.5% yield) of the product as a green powder (Figures S3,4). <sup>1</sup>H NMR (600 MHz,  $\text{CDCl}_3$ )  $\delta$  ppm: 7.73 (s, 1H), 7.46 (s, 1H), 6.94 (t,  $J$  = 7.8, 1H), 6.90, (dd,  $J$  = 8.1, 0.9, 1H), 6.43, (dd,  $J$  = 7.5, 0.9, 1H), 4.98 (s, 1H), 3.76 (s, 3H), 3.73 (s, 3H), 3.21 (m, 2H), 3.06 (m, 2H), 2.98 (m, 2H), 2.55 (m, 3H), 1.81 (m, 2H), 1.24 (m, 1H), 0.90 (t,  $J$  = 7.38, 3H). <sup>13</sup>C NMR (600 MHz,  $\text{CDCl}_3$ )  $\delta$  ppm: 168.73, 160.09, 149.42, 137.38, 133.69, 121.53, 116.12, 110.97, 106.22, 103.89, 103.46, 61.10, 60.73, 57.23, 53.10, 50.91, 40.18, 39.39, 29.43, 23.15, 18.63, 12.40. LRMS calcd for  $\text{C}_{22}\text{H}_{29}\text{N}_2\text{O}_4$  (ES-API+), 385.2; found, 385.1.

**Tert-butyl 4-(((2S,3S)-2-((E)-1,3-dimethoxy-3-oxoprop-1-en-2-yl)-3-ethyl-1,2,3,4,6,7,12,12b-octahydroindolo[2,3-a]quinolizin-8-yl)oxy)butanoate (3).**

A solution of *tert*-butyl 4-bromobutanoate (0.072 mL, 0.39 mmol, Combi-Blocks) was added dropwise over 30 min to a stirred solution of **2** (0.1 g, 0.26 mmol) and K<sub>2</sub>CO<sub>3</sub> (0.096 g, 0.58 mmol) in DMF (0.43 mL) at 60 °C and stirred for 12 h. The reaction was quenched with H<sub>2</sub>O and extracted three times with DCM. The combined extracts were washed with brine, dried over MgSO<sub>4</sub>, and concentrated into a dark yellow oil. The crude product was purified by prepacked amino-silica gel column chromatography (ethyl acetate/*n*-hexane 50:50–80:20) to give 66 mg (48% yield) of the product as a green oil (Figures S5,6). <sup>1</sup>H NMR (600 MHz, CDCl<sub>3</sub>) δ ppm: 7.44 (s, 1H), 6.99 (t, *J* = 7.9 Hz, 1H), 6.92 (d, *J* = 8.0 Hz, 1H), 6.45–6.41 (m, 1H), 4.08 (qt, *J* = 9.2, 6.1 Hz, 2H), 3.75 (s, 3H), 3.72 (s, 3H), 3.26–3.18 (m, 2H), 3.10 (tt, *J* = 18.2, 12.2 Hz, 4H), 2.72 (s, 1H), 2.64 (s, 1H), 2.62–2.53 (m, 2H), 2.49 (td, *J* = 7.4, 2.6 Hz, 2H), 2.16–2.07 (m, 2H), 1.95 (d, *J* = 13.4 Hz, 1H), 1.73 (s, 2H), 1.48 (s, 9H), 1.28–1.18 (m, 1H), 0.89 (t, *J* = 6.8 Hz, 3H). <sup>13</sup>C NMR (600 MHz, CDCl<sub>3</sub>) δ ppm: 172.38, 168.77, 160.07, 153.14, 136.85, 133.31, 121.37, 117.28, 111.05, 107.37, 103.69, 99.91, 79.83, 66.00, 61.83, 61.08, 57.30, 53.33, 50.89, 40.22, 39.44, 31.63, 29.50, 27.67, 24.57, 23.52, 18.64, 12.38. LRMS calcd for C<sub>30</sub>H<sub>43</sub>N<sub>2</sub>O<sub>6</sub> (ES-API+), 527.3; found, 527.3.

**4-(((2S,3S)-2-((E)-1,3-dimethoxy-3-oxoprop-1-en-2-yl)-3-ethyl-1,2,3,4,6,7,12,12b-octahydroindolo[2,3-a]quinolizin-8-yl)oxy)butanoic acid (Mit-hapten, 4).**

A solution of 10% TFA in DCM (0.361 mL) was added to a vial charged with **3** (0.02 g, 0.036 mmol) and allowed to stir for 18 h at rt. TFA was evaporated with DCM by nitrogen gas three times and the product was concentrated into 17.5 mg (98% yield) of a dark green oil (Figure S7). LRMS calcd for C<sub>26</sub>H<sub>35</sub>N<sub>2</sub>O<sub>6</sub> (ES-API+), 471.2; found, 471.2.

**Mit-BSA and Mit-FliC.**

Mit-hapten (**4**) (1 mg, 2.35 μmols) was mixed with EDC (4.5 mg, 23 μmols), NHS (2.7 mg, 23 μmols), and TEA (1 μL, 4.7 μmols) in DMF (0.85 mL) and water (15 μL) for 1 h or until fully activated. Activation was monitored by LC/MS. BSA or FliC (1 mg, 15 or 18 nmols, respectively) was added to activated hapten and brought to a final volume of 1 mL in PBS, pH 7.4 and the reaction solution stirred overnight at 5 °C. Protein immunoconjugates were purified by dialysis in PBS, pH 7.4, and characterized by MALDI (copy number = 19 for BSA, 7 for FliC, (Figures S10–13). Unconjugated FliC = 55481 g/mols.

**7-Hydroxymitragynine.**

A solution of [bis(trifluoroacetoxy)-iodo]benzene (PIFA, 0.119 g, 0.028 mmol) in acetonitrile (1.062 mL) was added dropwise to a stirred solution of mitragynine (0.1 g, 0.025 mmol) in acetonitrile (3.585 mL) and water (1.255 mL) at 0 °C under argon, and stirred for 3 h or until reaction completion.<sup>17</sup> The reaction was quenched with cold sat. NaHCO<sub>3</sub> (aq.) and extracted three times with chloroform. The combined extracts were washed with brine, dried over MgSO<sub>4</sub>, and concentrated into a yellow oil. The residue was purified by prepacked amino-silica gel column chromatography (ethyl acetate/*n*-hexane 30:70–50:50) to give 25 mg (40% yield) of 7-hydroxymitragynine as a pale yellow crystalline product (Figures S8,9). <sup>1</sup>H NMR (600 MHz, CDCl<sub>3</sub>) δ ppm: 7.44 (s, 1H), 7.29 (t, *J* = 7.8 Hz, 1H),

7.20 (d,  $J=7.8$  Hz, 1H), 6.72 (d,  $J=8.4$  Hz, 1H), 5.31 (s, 1H), 3.86 (s, 3H), 3.81 (s, 3H), 3.69 (s, 3H), 3.13 (dd,  $J=11.1, 2.7$ , 1H), 3.05 (dd,  $J=11.4, 1.8$ , 1H), 3.01 (dt,  $J=13.8, 3.6$ , 1H), 2.81 (m, 2H), 2.64 (m, 1H), 2.49 (dd,  $J=11.4, 2.4$ , 1H), 1.88 (dt,  $J=14, 2.6$ , 1H), 1.67 (m, 3H), 1.26 (m, 2H), 0.83 (t,  $J=7.5$  Hz, 3H).  $^{13}\text{C}$  NMR (600 MHz,  $\text{CDCl}_3$ )  $\delta$  ppm: 183.83, 168.82, 160.26, 155.43, 154.57, 113.75, 110.80, 108.41, 90.54, 61.31, 61.02, 57.69, 55.92, 55.01, 50.82, 49.57, 40.06, 38.83, 35.33, 29.24, 25.61, 18.49, 12.36. MS calcd for  $\text{C}_{23}\text{H}_{31}\text{N}_2\text{O}_5$  (ES-API+), 415.2; found, 415.3.

### Animals.

All studies were performed in compliance with the Scripps Institutional Animal Care and Use Committee and all protocols adhered to the National Institute of Health Guide for the Care and Use of Laboratory Animals. Mice were group-housed in an AAALAC-accredited vivarium containing temperature and humidity controlled rooms and kept on a reverse light cycle (lights on: 9 PM–9 AM). All behavioral procedures were performed during the dark phase.

### Lethality.

A sample size of six mice per dose was the minimum number of animals necessary to determine an approximate  $\text{LD}_{50}$  and prevent unnecessary repetition. All doses were administered as a bolus retro-orbital intravenous injection and mice were monitored over 24 h for overdose.<sup>18</sup> Mitragynine and 7-hydroxymitragynine have low solubility in aqueous solution (Table S4), so the compounds were first dissolved in a 50% tween/DMSO solution, then diluted to 90% saline.<sup>19</sup> With this vehicle, we were at the limit of solubility at the highest doses tested. The doses for mitragynine were 62, 31, 25, 15, and 8 mg/kg (Figure S14). For 7-hydroxymitragynine, the doses were 50, 25, 12.5, and 6.25 mg/kg (Figure S15). For direct comparison to iv heroin potency, we also performed a lethality assay with heroin (40, 20, 10, and 5 mg/kg) at the same time as mitragynine and 7-hydroxymitragynine lethality assays (Figure S16). We wanted to compare iv to oral lethality for the two alkaloids of Kratom, so we also determined an approximate oral  $\text{LD}_{50}$  value for mitragynine using the following doses: 500, 250, 125, and 62.5 mg/kg (Figure S17). We attempted to determine an oral  $\text{LD}_{50}$  value for 7-hydroxymitragynine; however, none of the mice expired at any of the doses (50, 25, 12.5, and 6.25 mg/kg; Figure S18).

### mAb Development.

Female A/J mice (Jackson Laboratories; 7 weeks old;  $n=4$ ) were immunized intraperitoneally (ip) with 50  $\mu\text{g}$  of immunoconjugate vaccines (Mit-FliC conjugate, CpG ODN 1826, and alum) on days 0, 20, and 61. The vaccination schedule can be seen in Table 1. Mice were bled on day 27 and 68 using retro-orbital puncture in order to collect approximately 100–150  $\mu\text{L}$  of whole blood. Antibody titers were analyzed by enzyme-linked immunosorbent assay (ELISA). A final tail vein iv injection of Mit-FliC conjugate (50  $\mu\text{g}$ ) in PBS (75  $\mu\text{L}$ ) was administered one month after the final boost. After 3 days, the spleen was fused with a myeloma cell line to produce hybridomas according to standard techniques.<sup>20</sup> The hybridomas were plated into 15 96-well plates and screened against Mit-BSA conjugate by ELISA after 2 weeks. Each member of a final panel of 32 mAbs was then assessed for binding to mitragynine by SPR (Table S1).

## ELISA.

Plates (96-well Costar 3690) were coated with Mit-BSA diluted in PBS pH 7.4 (10  $\mu\text{g}/\text{mL}$ , 25  $\mu\text{L}/\text{well}$ ) and incubated at 4 °C overnight in a moist chamber. The plates were washed five times with deionized water and blocked with 5% nonfat powdered milk in PBS pH 7.4 (50  $\mu\text{L}/\text{well}$ ) at rt for 15 min. Plasma samples, diluted in 10% fetal calf serum (FCS) media, were serially diluted 2-fold across plate in 10% FCS media. Plates were incubated at 37 °C for 2 h, washed with H<sub>2</sub>O, and treated with secondary antibody (goat-antimouse IgG (H+L)-HRP, Southern Biotech, catalogue no. 1030-05, diluted 1:1000 in 5% nonfat powdered milk in PBS pH 7.4, 25  $\mu\text{L}/\text{well}$ ). Plates were incubated at 37 °C for 30 min, washed with H<sub>2</sub>O, treated with developing reagent (ABTS, ROCHE 10102946001; 0.3 mg/mL in 0.1 M citrate, pH 4, with 2 mM H<sub>2</sub>O<sub>2</sub>; 200  $\mu\text{L}/\text{well}$ ), and incubated at room temperature for 30 min. Plates were read on a SpectraMax 190 (Molecular Devices, Sunnyvale, CA) at 405 nm. Midpoint titer was calculated by taking the inverse of the dilution at which the absorbance was 50% of the max value.

## Surface Plasmon Resonance (SPR).

The binding IC<sub>50</sub> for mouse serum IgGs and free mitragynine or 7-hydroxymitragynine was determined by competitive binding assay via SPR using a Biacore 3000 instrument (GE Healthcare) equipped with a research-grade CM5 sensor chip according to literature methods.<sup>8</sup> Diluted mouse serum from day 24 and 38 were incubated with serial dilutions of mitragynine and 7-hydroxymitragynine and injected into a Biacore 3000 containing a Mit-BSA-loaded sensor chip. The ligand, BSA immunoconjugate, was immobilized using NHS, EDC coupling reaction. The surface of flow cells 1 and 2 were activated for 7 min with a 1:1 mixture of 0.1 M NHS and 0.1 M EDC at a flow rate of 5  $\mu\text{L}/\text{min}$ . The ligand resuspended in 10 mM sodium acetate (pH 4.0) was immobilized at a density of 5,000 RU on flow cell 2; whereas flow cell 1 was immobilized with BSA at the same density to serve as a reference surface. All the surfaces were blocked with a 7 min injection of 1.0 M ethanolamine-HCl (pH 8.5). The mouse serum IGs were diluted in running buffer (HBS-EP + buffer) and titrated on both coated flow cells, so as to give a response of ~100 RU within 3 min of injection and 2.5 min dissociation at a flow rate of 30  $\mu\text{L}/\text{min}$ . The mouse serum IGs prepared in HBS-EP + buffer at determined concentration was incubated with a series concentration of compounds for 20 min at rt before conducting the competitive binding assay. The chip surface was regenerated by injection of 10 mM Gly-HCl (pH 1.5) for 30 s before the next round of assays. IC<sub>50</sub> values were determined from a 6-point mitragynine dilution and curve and derived from a nonlinear fit of the binding curves in PRISM 6.

## Competitive ELISA.

Plates (96-well Costar 3690) were coated with Mit-BSA diluted in PBS pH 7.4 (5  $\mu\text{g}/\text{mL}$ , 25  $\mu\text{L}/\text{well}$ ) and incubated at 37 °C overnight. Then, plates were fixed with MeOH (50  $\mu\text{L}/\text{well}$ ) at room temperature for 5 min, blocked with 5% nonfat powdered milk in PBS pH 7.4 (50  $\mu\text{L}/\text{well}$ ) 37 °C for 30 min, and charged with either 0.5–10  $\mu\text{g}/\text{mL}$  mitragynine in 2% BSA in PBS pH 7.4 or urine samples containing 1–3  $\mu\text{g}/\text{mL}$  (15  $\mu\text{L}/\text{well}$ ). Hybridoma supernatants were plated at 1:400 dilution (diluted in 2% BSA in PBS pH 7.4, 15  $\mu\text{L}/\text{well}$ ). Plates were incubated at 37 °C for 60 min, washed with H<sub>2</sub>O, and treated with secondary

antibody (donkey-antimouse Ig(H+L)-HRP, Southern Biotech, catalogue no. 3010–05, diluted 1:10,000 in 2% BSA in PBS pH 7.4, 25  $\mu\text{L}$ /well). Plates were incubated at 37 °C for 30 min, washed with  $\text{H}_2\text{O}$ , treated with developing reagent (TMB Pierce Substrate Kit, 50  $\mu\text{L}$ /well), and incubated at room temperature in the dark for 10–20 min. Color development was halted by addition of 2 M  $\text{H}_2\text{SO}_4$  (50  $\mu\text{L}$ /well) and plates were read on a SpectraMax M2e (Molecular Devices, Sunnyvale, CA) at 450 nm. Results for the competitive ELISA are given in Table S2.

### Lateral Flow Detection Assay.

Lateral flow strips were constructed with Lohmann Precision Die Cutting (GL-57065) backing cards, Ahlstrom (8950) conjugate pads, Ahlstrom (222) wick pads, and Millipore (C048) sample pads. Monoclonal antibodies (10  $\mu\text{g}$ ) were conjugated to gold nanoparticles (ABIOX - CG40, 40 nM, 1.5 mL) by mixing for 15 min with (15  $\mu\text{L}$  0.2 M  $\text{K}_2\text{CO}_3$ ), followed by blocking with 2% BSA (50  $\mu\text{L}$ ) and allowing to mix for an additional 15 min. Antibody-conjugated gold nanoparticles were purified by centrifuging at 12,000 rpm for 5 min, removing supernatant, and resuspending in 0.3 mL storage solution (5 mM borate buffer, pH 8, with 0.1% BSA, 0.15% Tween-20, and 5% sucrose). The absorbance of the gold solution was read and volume was adjusted until OD = 5. During the crude screen of monoclonals, MIT11C2, MIT17B7, MIT29B7, and MIT25G11 were tested against 0  $\mu\text{g}/\text{mL}$  and 10  $\mu\text{g}/\text{mL}$  mitragynine with MIT11C2, MIT29B7, and MIT25G11 performing the best, that is, showing the greatest difference between blank and the concentration sample. For each crude test, 1  $\mu\text{L}$  of Mit-BSA at 0.5 mg/mL was loaded in the test area and 5  $\mu\text{L}$  of antibody-conjugated gold nanoparticles was loaded on the sample pad. Lateral flow strips were then optimized with the purified, subcloned antibodies, MIT11C2 and MIT29B7, with MIT29B7 performing the best. In optimizing lateral flow strips, 2, 1, and 0.5  $\mu\text{L}$  of Mit-BSA was tested at 0.5, 0.3, and 0.25 mg/mL. The optimal amount of Mit-BSA was 0.5  $\mu\text{L}$  at 0.3 mg/mL. In preparing the lateral flow strips, 5 and 2.5  $\mu\text{L}$  of antibody-conjugated gold nanoparticles were tested with 5  $\mu\text{L}$  performing the best. For each optimization test, the strip was run with mitragynine at 10, 1, 0.5, and 0  $\mu\text{g}/\text{mL}$ . The final optimized lateral flow strips were analyzed in triplicate with mitragynine and 7-hydroxymitragynine at 10, 1, and 0.5  $\mu\text{g}/\text{mL}$  for MIT29B7. In translating the strips for detection of urine samples, several buffering techniques were explored to balance the pH of the urine samples. Spiked urine containing 10  $\mu\text{g}/\text{mL}$  mitragynine and blank urine containing no mitragynine was used to analyze the efficiency of these buffering techniques. Urine samples were diluted 1:1, 1:2, or 1:3 with PBS, pH 7.4, and run on optimized strips; however, none of these conditions gave results similar to that of buffer samples. Lateral flow strips were preloaded with 15, 35, or 75  $\mu\text{L}$  of PBS, pH 7.4, or 15, 35, or 75  $\mu\text{L}$  of 10 $\times$  PBS, pH 7.4, and then test samples were applied. Of these conditions, 15  $\mu\text{L}$  of 10 $\times$  PBS, pH 7.4 preloaded onto the strips performed closest to that of buffer samples and was used for the remaining urine strips. Next, a standard curve was obtained for mitragynine and 7-hydroxymitragynine at 2, 1, 0.5, 0.25, 0.125, and 0  $\mu\text{g}/\text{mL}$  in urine. Samples were allowed to run on the lateral flow strips and dry completely then were read on the Leelu Benchtop Reader (Lumos Diagnostics) with red/green illumination. The background subtracted measurement of the visual intensity of the test spot is reported as “peak height,” with the background measurement occurring 50–100 points to the left or right of the peak. An image of a strip with its corresponding peak

measurement can be found in Figure S19 as an example of the read-out data. Curves were fit with a one-phase exponential decay model. To validate the curves, two urine samples containing concentrations of mitragynine or 7-hydroxymitragynine unknown to the investigator (operator-blind) were analyzed by the lateral flow strips. The percent error for the predicted concentrations were calculated using the following equation

$$\frac{\text{Predicted Concentration} - \text{Actual Concentration}}{\text{Actual Concentration}} \times 100$$

## RESULTS AND DISCUSSION

As a segue to our mitragynine lateral flow development, we investigated Kratom's potential therapeutic risks. Although it has been promoted as an alternative medicine for opioid substance use disorder, Kratom use has been associated with psychosis, seizures, and even death.<sup>21</sup> The latter of which little is known based on allometric scaling of Kratom's psychoactive alkaloid constituents. Mitragynine, 7-hydroxymitragynine, and heroin were evaluated head-to-head in a lethality assay using male Swiss Webster mice (Table 1). Surprisingly, these data reveal that mitragynine and 7-hydroxymitragynine have similar toxicity to heroin when administered intravenously (iv). Mice appeared to expire from respiratory depression after receiving a bolus iv injection of mitragynine or 7-hydroxymitragynine, with most overdose events occurring within the first 10 min of drug exposure (Figures S14–16). This observation conflicts with the observations from Kruegel et. al that mitragynine is a competitive antagonist at the murine  $\mu$ -OR.<sup>13</sup> Although seizure events were not measured in this experiment, they were observed for many of the surviving mice within the first 20 min of drug administration.

It is widely believed that opioid induced respiratory depression is mediated by the  $\mu$ -OR and several mitragynine derivatives have been identified as  $\mu$ -OR agonists. Our lethality studies suggest that mitragynine agonism at the  $\mu$ -OR may contribute to its lethality in mice, despite conflicting reports.<sup>8,9,12,13</sup> A lethality rescue experiment with naloxone, a known  $\mu$ -OR antagonist, would further support this theory. Interestingly, in a recent self-administration study in rats, it was found that both a  $\mu$ -OR antagonist (naloxonazine) and a  $\delta$ -OR antagonist (naltrindole) were required to reduce 7-hydroxymitragynine self-administration.<sup>23</sup> The  $\mu$ -OR antagonist alone did not reduce 7-hydroxymitragynine intake, indicating that several receptors may be at play for the mitragynine family of compounds. In this case, lethality studies should be conducted with a variety of OR antagonists. McCurdy and colleagues also showed that mitragynine self-administration reduced subsequent morphine intake, demonstrating mitragynine's potential for therapeutic use. This self-administration model also highlighted the possibility of abuse of 7-hydroxymitragynine. It is possible that mitragynine has a different mechanism of action at therapeutic versus lethal doses, or that multiple ORs are involved in its lethality.

Kratom leaves are typically chewed or crushed in warm water and consumed as a "tea."<sup>21</sup> Thus, we investigated how the oral LD<sub>50</sub> values directly compared to the acquired iv values for mitragynine and 7-hydroxymitragynine (Figure S17–18). Indeed, we observed an LD<sub>50</sub> value for mitragynine within the reported range through oral administration (Table 1).



Although 7-hydroxymitragynine is reported to have 50 times the potency of mitragynine at the receptor level, we failed to observe any deaths at oral doses up to one-tenth the oral LD<sub>50</sub> dose of mitragynine. Because no mice expired, we were unable to fit a lethality curve to calculate an LD<sub>50</sub>. We posit that this difference in oral lethality is either due to a unique difference in potency or oral absorption variation in Swiss Webster mice. Although no bioavailability studies have been done in mice, there is some discrepancy between mitragynine and 7-hydroxymitragynine absorption and stability in cellular assays (Table S5).<sup>19,24,25</sup> Interestingly, one study found that 7-hydroxymitragynine is converted to mitragynine (45%) in human liver microsomes over a 2 h incubation.<sup>24</sup> It is important to note that although no deaths were observed, severe respiratory depression and seizures were observed in mice receiving oral 7-hydroxymitragynine. Given the unanticipated lethality seen with Kratom alkaloid constituents, increasing therapeutic value of mitragynine, and abuse potential for 7-hydroxymitragynine, a simple, efficient detection method for Kratom is now of greater importance.

The first step toward lateral flow assay development involves design of a hapten capable of producing exceptional-binding monoclonal antibodies. Selection of a linker position in hapten design is essential in obtaining antibodies with affinity to the parent drug. The structure of mitragynine offers several locations and strategic connections to a carrier protein, including an amide-linkage through the C16 ester on ring D and an alkyl linkage at the indole amine on ring B. In this study, ether linkage on ring A of mitragynine was selected to preserve the chemical characteristics of the drug. This was achieved in three steps starting from commercially available mitragynine (Scheme 1). Selective demethylation of **1** at the ring A ether was achieved using a hard acid and soft nucleophile system.<sup>13,26</sup> Alkylation of the crude phenol with tert-butyl 4-bromobutanoate was then undertaken to yield the t-butyl protected hapten **3** in modest yield. Deprotection with 10% TFA in dichloromethane (DCM) gave the desired “Mit”-hapten (**4**). Bioconjugation of hapten to carrier proteins BSA and FliC proceeded with EDC and sulfo-NHS to generate Mit-BSA and the Mit-FliC immunoconjugates. The carrier protein FliC (bacterial flagellin) was selected for this study because of its previous demonstration to produce excellent antihapten immune response with our cocaine vaccine.<sup>27</sup> The immuno-conjugates were then formulated with the oligonucleotide CpG<sup>28</sup> and alum adjuvants for vaccination in mice.

Sera collected from mice at week 3 and 5 were analyzed by ELISA against Mit-BSA to determine the presence of antimitragynine antibodies (Table 2). As expected, the mit-vaccine exhibited robust midpoint titer levels in each individual mouse. Titer levels appeared to remain constant from week 3 to 5, so an additional boost was added to the immunization schedule at week 6. Unfortunately, titers did not increase with the added boost. Mice 1 and 2 were selected for spleen harvest and subsequent fusion with immortal myeloma cells at week 10, yielding 32 mAbs that showed affinity to Mit-BSA by ELISA with midpoint titers ranging from 64–2048 (Table S1). All 32 monoclonals were screened for binding to mitragynine against Mit-BSA by SPR with IC<sub>50</sub>s ranging from 0.1 - > 10  $\mu$ M (Table S1).

Competitive ELISA was selected as a suitable screening assay as it exhibits a comparable binding mechanism to that of a lateral flow assay. All of the mAbs exhibiting potent (0.1–1  $\mu$ M) and modest (~1  $\mu$ M) binding were examined in competitive ELISA in the presence of

buffer and urine to determine solution effect on antibody performance (Table S2). Monoclonal antibodies MIT11C2 (isotype  $\kappa$ ,  $\lambda$ ,  $\gamma$ 1,  $\gamma$ 2b,  $\gamma$ 3), MIT17B7 (isotype  $\kappa\gamma$ 1, 2b), and MIT29B7 (isotype  $\kappa\gamma$ 1) exhibited the tightest binding to mitragynine as determined by surface plasmon resonance (SPR, Table 2). These mAbs along with a medium (MIT25G11, isotype  $\kappa\gamma$ 1) and low (MIT17H11, isotype  $\kappa\gamma$ 1) affinity mAb with were also selected for further characterization in a crude lateral flow test (Table 3). In the competitive ELISA screen, MIT17B7, MIT29B7, and MIT17H11 performed similarly in buffer and urine, whereas the IC<sub>50</sub> values for the other two mAbs in each solution differed by ~10-fold.

On the basis of this data, crude mAbs were tested for strip performance to determine which antibodies had the greatest differentiation between a control (0  $\mu$ g/mL mitragynine) and a concentrated sample (10  $\mu$ g/mL mitragynine) of drug. MIT17H11 exhibited poor binding to the gold nanoparticles and did not undergo further evaluation. As a simple metric in this preliminary test, a blank response was scored “10” while the absence of color from the mAb conjugated gold nanoparticles was scored “0”. MIT17B7 exhibited no binding during lateral flow. Moreover, MIT11C2, MIT29B7, and MIT25G11 showed good distinction between samples, particularly MIT29B7. Taking each screening parameter (midpoint titer, SPR IC<sub>50</sub>, competitive ELISA IC<sub>50</sub> in urine and buffer, and crude strip performance) into account, MIT11C2 and MIT29B7 were selected for subcloning.

The binding affinity of the final purified mAbs to mitragynine and 7-hydroxymitragynine were characterized by SPR (Table 4). Both antibodies exhibit nanomolar binding to mitragynine and 7-hydroxymitragynine, with MIT29B7 showing superior affinity for both drugs. In considering antibody binding characteristics necessary for lateral flow, specificity/affinity to the BSA conjugate is essential for a strong negative signal. Furthermore, affinity to the free drug must be greater than that of the BSA conjugate to ensure a clear band for positive tests. Based on these criteria, MIT11C2 was eliminated as a candidate for further development.

This sequence of events led to MIT29B7's selection for final optimization on lateral flow strips with the goal of a 500 ng/mL cutoff in buffer. This goal was determined based on the reported urine concentrations of mitragynine in post-mortem toxicology reports of overdose deaths involving Kratom, which range from 0.167 to 1.2  $\mu$ g/mL (Table S3).<sup>4,5,29–31</sup> Several conditions at each position of the testing strip were analyzed with the final conditions being 150 ng Mit-BSA on the testing position and 170  $\mu$ g mAb conjugated to gold nanoparticles loaded onto the sample pad. A last hurdle included obtaining a standard curve for mitragynine and 7-hydroxymitragynine. Lateral flow strips were run in triplicate and read on a benchtop reader reporting the visible intensity of the test spot as “peak height” (example readout, Figure S19). The results can be seen in Figure 3A and B, with the 500 ng/mL concentration marked by a dotted line. All concentrations above 500 ng/mL were at essentially background levels, whereas concentration levels below 500 ng/mL were in the linear range of the curve. Moreover, for concentrations  $\geq$  500 ng/mL this lateral flow immunoassay could act as a qualitative detection assay, whereas for concentrations <500 ng/mL the assay could be used for quantitative detection.

On the basis of the strip performance of MIT29B7, it was used for analysis of drug in human urine samples. Here, a standard curve from human urine samples containing mitragynine or 7-hydroxymitragynine ranging from 0.16 to 5  $\mu\text{g}/\text{mL}$  was obtained. In translating the strips for use with human urine, several buffer preloading techniques were examined to ensure that the final testing solution had a balanced pH. We found that our strips performed the best with human urine samples when the sample pad was preloaded with 10x PBS, pH 7.4 (15  $\mu\text{L}$ ).

Mitragynine binding to MIT29B7 in urine appears to parallel the simple buffer system, albeit with greater variability, as was predicted by SPR (Figure 3C). Unanticipatedly, the strips showed no difference in signal between 7-hydroxymitragynine or blank urine samples (Figure S20). However, this finding is not a detriment to the utility of the test strip. Because the whole leaf of kratom is typically consumed and abused, it is only essential that a diagnostic tool for human samples be able to detect one of its metabolites.

Accordingly, the lateral flow assay was then challenged in a user-blind measurement test. In this test, two urine samples containing concentrations of mitragynine unknown to the operator were measured, then their concentrations were back calculated using the urine standard curve (Figure 3D). The peak height recorded for blind sample A was out of range for the standard curve. However, it was within the range of peak heights observed for the 2  $\mu\text{g}/\text{mL}$  samples and was predicted to be 2  $\mu\text{g}/\text{mL}$ . Indeed, the samples actual concentration was 1.3  $\mu\text{g}/\text{mL}$ ; these results are in line with a 0.5  $\mu\text{g}/\text{mL}$  cutoff. The peak height for blind sample B on the other hand was within the range of the standard curve and was predicted to be 0.24  $\mu\text{g}/\text{mL}$ . Moreover, its actual concentration was 0.3  $\mu\text{g}/\text{mL}$ , which puts our prediction within 20% error. Considering that 0.3  $\mu\text{g}/\text{mL}$  is approaching our 0.5  $\mu\text{g}/\text{mL}$  cutoff this was viewed as an acceptable finding.

## CONCLUSION

Mitragynine and 7-hydroxymitragynine, the two major alkaloids found in the pharmacologically active plant Kratom appear to have similar potency to each other and to heroin in Swiss Webster mice. This is surprising considering the existing opioid receptor potency data for the two Kratom alkaloids and sheds light on the need for additional research on these two drugs. In this study, we detailed the synthesis of a mitragynine hapten which led to the production of two monoclonal antibodies, MIT11C2 and MIT29B7, both of which exhibited nanomolar binding to mitragynine and 7-hydroxymitragynine. We presented their development in a lateral flow assay with a detection cut off of 500 ng/mL. On the basis of our findings, the assay could be developed as a qualitative tool to detect the presence or absence of mitragynine or 7-hydroxymitragynine in nonbiological solutions. In contrast, for nonbiological solutions at concentrations <500 ng/mL, these lateral flow strips could be developed into a quantitative detection device. With further refinement, the assay will undoubtedly be an asset to law enforcement agents and health care providers as Kratom gains popularity in the U.S. and as the opioid crisis evolves and continues.

## Supplementary Material

Refer to Web version on PubMed Central for supplementary material.

## ACKNOWLEDGMENTS

The authors would like to thank Professor Atsushi Kimishimi (Osaka University) and Elena de Orbe Izquierdo (Institut Català d'Investigació Química) for synthesis advice. The authors are especially grateful to Lumos Diagnostics for access to their Leelu Benchtop Reader. This is manuscript #29739 from The Scripps Research Institute.

### Funding

This work was supported by the National Institute of Health under Grant UH3DA041146 and the Skaggs Institute for Chemical Biology.

## ABBREVIATIONS

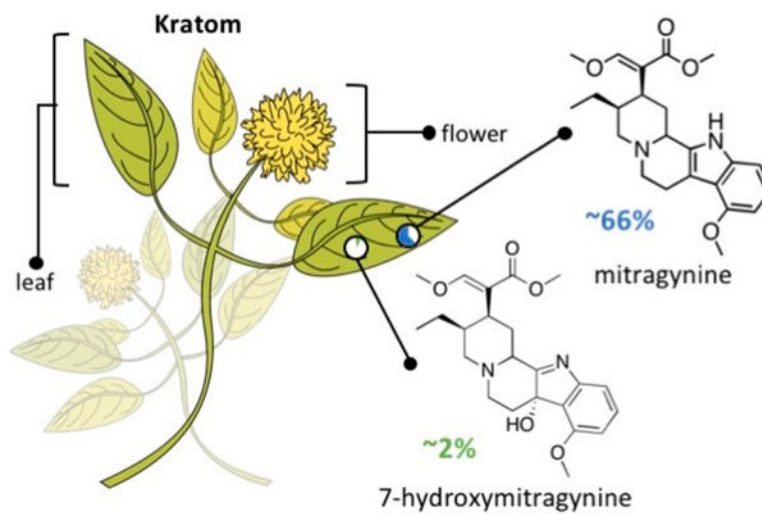
<b>GTP</b>	guanosine triphosphate
<b>cAMP</b>	cyclic adenosine monophosphate
<b>CpG ODN</b>	cytosine-phosphodiester-guanine oligodeoxynucleotide
<b>PBS</b>	phosphate-buffered saline
<b>EDC</b>	1-ethyl-3-(3-(dimethylamino)propyl)carbodiimide
<b>MALDI-ToF MS</b>	matrix-assisted laser desorption ionization time-of-flight mass spectrometry
<b>s.c.</b>	subcutaneous
<b>ip</b>	intraperitoneal
<b>iv</b>	intravenous
<b>SPR</b>	surface plasmon resonance
<b>DCM</b>	dichloromethane
<b>TEA</b>	trimethylamine
<b>DMF</b>	dimethylformamide
<b>TFA</b>	trifluoroacetic acid
<b>PIFA</b>	[[bis(trifluoroacetoxy)-iodo]]benzene

## REFERENCES

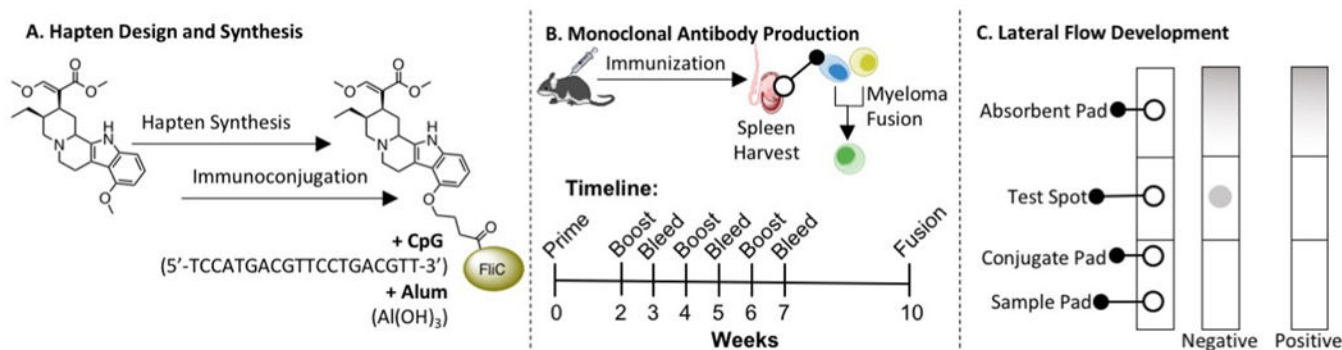
- (1). Cinosi E, Martinotti G, Simonato P, Singh D, Demetrovics Z, Roman-Urrestarazu A, Bersani FS, Vicknasingam B, Piazzon G, Li JH, Yu WJ, Kapitany-Foveny M, Farkas J, Di Giannantonio M, and Corazza O (2015) Following “the Roots” of Kratom (*Mitragyna speciosa*): The Evolution of an Enhancer from a Traditional Use to Increase Work and Productivity in Southeast Asia to a Recreational Psychoactive Drug in Western Countries. *BioMed Res. Int.* 2015, 1.

- Author Manuscript
- Author Manuscript
- Author Manuscript
- Author Manuscript
- (2). Hassan Z, Muzaimi M, Navaratnam V, Yusoff NH, Suhaimi FW, Vadivelu R, Vicknasingam BK, Amato D, von Horsten S, Ismail NI, Jayabalan N, Hazim AI, Mansor SM, and Muller CP (2013) From Kratom to mitragynine and its derivatives: physiological and behavioural effects related to use, abuse, and addiction. *Neurosci. Biobehav. Rev.* 37 (2), 138–51. [PubMed: 23206666]
  - (3). Chang-Chien GC, Odonkor CA, and Amorapanth P (2017) Is Kratom the New ‘Legal High’ on the Block?: The Case of an Emerging Opioid Receptor Agonist with Substance Abuse Potential. *Pain Physician* 20 (1), E195–E198. [PubMed: 28072812]
  - (4). Holler JM, Vorce SP, McDonough-Bender PC, Maglulio J Jr., Solomon CJ, and Levine B (2011) A drug toxicity death involving propylhexedrine and mitragynine. *J. Anal. Toxicol.* 35 (1), 54–9. [PubMed: 21219704]
  - (5). Domingo O, Roider G, Stover A, Graw M, Musshoff F, Sachs H, and Bicker W (2017) Mitragynine concentrations in two fatalities. *Forensic Sci. Int.* 271, e1–e7. [PubMed: 28089300]
  - (6). Gottlieb S Statement from FDA Commissioner Scott Gottlieb, M.D., on the agency’s scientific evidence on the presence of opioid compounds in kratom, underscoring its potential for abuse;. FDA: 2018.
  - (7). Administration, U. S. F. a. D. FDA Investigates Multistate Outbreak of Salmonella Infections Linked to Products Reported to Contain Kratom. 2018.
  - (8). Stott DG, and Pleuvry BJ (1991) Relationship between analgesia and respiratory depression for mu opioid receptor agonists in mice. *Br. J. Anaesth.* 67 (5), 603–7. [PubMed: 1684279]
  - (9). Boom M, Niesters M, Sarton E, Aarts L, Smith TW, and Dahan A (2012) Non-analgesic effects of opioids: opioid-induced respiratory depression. *Curr. Pharm. Des.* 18 (37), 5994–6004. [PubMed: 22747535]
  - (10). Matsumoto K, Mizowaki M, Suchitra T, Takayama H, Sakai S, Aimi N, and Watanabe H (1996) Antinociceptive action of mitragynine in mice: evidence for the involvement of supraspinal opioid receptors. *Life Sci.* 59 (14), 1149–55. [PubMed: 8831802]
  - (11). Takayama H, Ishikawa H, Kurihara M, Kitajima M, Aimi N, Ponglux D, Koyama F, Matsumoto K, Moriyama T, Yamamoto LT, Watanabe K, Murayama T, and Horie S (2002) Studies on the synthesis and opioid agonistic activities of mitragynine-related indole alkaloids: discovery of opioid agonists structurally different from other opioid ligands. *J. Med. Chem.* 45 (9), 1949–56. [PubMed: 11960505]
  - (12). Varadi A, Marrone GF, Palmer TC, Narayan A, Szabo MR, Le Rouzic V, Grinnell SG, Subrath JJ, Warner E, Kalra S, Hunkele A, Pagirsky J, Eans SO, Medina JM, Xu J, Pan YX, Borics A, Pasternak GW, McLaughlin JP, and Majumdar S (2016) Mitragynine/Corynantheidine Pseudoindoxyls As Opioid Analgesics with Mu Agonism and Delta Antagonism, Which Do Not Recruit beta-Arrestin-2. *J. Med. Chem.* 59 (18), 8381–97. [PubMed: 27556704]
  - (13). Kruegel AC, Gassaway MM, Kapoor A, Varadi A, Majumdar S, Filizola M, Javitch JA, and Sames D (2016) Synthetic and Receptor Signaling Explorations of the Mitragyna Alkaloids: Mitragynine as an Atypical Molecular Framework for Opioid Receptor Modulators. *J. Am. Chem. Soc.* 138 (21), 6754–64. [PubMed: 27192616]
  - (14). Matsumoto K, Horie S, Ishikawa H, Takayama H, Aimi N, Ponglux D, and Watanabe K (2004) Antinociceptive effect of 7-hydroxymitragynine in mice: Discovery of an orally active opioid analgesic from the Thai medicinal herb *Mitragyna speciosa*. *Life Sci.* 74 (17), 2143–55. [PubMed: 14969718]
  - (15). Limsuwanchote S, Wungsintaweekul J, Keawpradub N, Putalun W, Morimoto S, and Tanaka H (2014) Development of indirect competitive ELISA for quantification of mitragynine in Kratom (*Mitragyna speciosa* (Roxb.) Korth.). *Forensic Sci. Int.* 244, 70–7. [PubMed: 25216455]
  - (16). Limsuwanchote S, Putalun W, Tanaka H, Morimoto S, Keawpradub N, and Wungsintaweekul J (2017) Development of an immunochromatographic strip incorporating anti-mitragynine monoclonal antibody conjugated to colloidal gold for kratom alkaloids detection. *Drug Test Anal.*
  - (17). Takayama H, Misawa K, Okada N, Ishikawa H, Kitajima M, Hatori Y, Murayama T, Wongseripatana S, Tashima K, Matsumoto K, and Horie S (2006) New procedure to mask the 2,3-pi bond of the indole nucleus and its application to the preparation of potent opioid receptor agonists with a Corynanthe skeleton. *Org. Lett.* 8 (25), 5705–8. [PubMed: 17134252]

- (18). Yardeni T, Eckhaus M, Morris HD, Huizing M, and Hoogstraten-Miller S (2011) Retro-orbital injections in mice. *Lab Anim (NY)* 40 (5), 155–60. [PubMed: 21508954]
- (19). Ramanathan S, Parthasarathy S, Murugaiyah V, Magosso E, Tan SC, and Mansor SM (2015) Understanding the physicochemical properties of mitragynine, a principal alkaloid of *Mitragyna speciosa*, for preclinical evaluation. *Molecules* 20 (3), 4915–27. [PubMed: 25793541]
- (20). Ozato K, Mayer N, and Sachs DH (1980) Hybridoma cell lines secreting monoclonal antibodies to mouse H-2 and Ia antigens. *J. Immunol* 124 (2), 533–40. [PubMed: 7188699]
- (21). Chien GCC, Odonkor C, and Amoranpanth P (2017) Is Kratom the new ‘legal high’ on the block?: The case of an emerging opioid receptor agonist with substance abuse potential. *Pain physician* 20, E195–E198. [PubMed: 28072812]
- (22). Sabetghadam A, Navaratnam V, and Mansor SM (2013) Dose–Response Relationship, Acute Toxicity, and Therapeutic Index between the Alkaloid Extract of *Mitragyna speciosa* and Its Main Active Compound Mitragynine in Mice. *Drug Dev. Res.* 74 (1), 23–30.
- (23). Hemby SE, McIntosh S, Leon F, Cutler SJ, and McCurdy CR (2018) Abuse liability and therapeutic potential of the *Mitragyna speciosa* (kratom) alkaloids mitragynine and 7-hydroxymitragynine. *Addict Biol.*,
- (24). Manda VK, Avula B, Ali Z, Khan IA, Walker LA, and Khan SI (2014) Evaluation of in vitro absorption, distribution, metabolism, and excretion (ADME) properties of mitragynine, 7-hydroxymitragynine, and mitraphylline. *Planta Med.* 80 (7), 568–76. [PubMed: 24841968]
- (25). Parthasarathy S, Ramanathan S, Ismail S, Adenan MI, Mansor SM, and Murugaiyah V (2010) Determination of mitragynine in plasma with solid-phase extraction and rapid HPLC-UV analysis, and its application to a pharmacokinetic study in rat. *Anal. Bioanal. Chem.* 397 (5), 2023–30. [PubMed: 20454783]
- (26). Fuji K, Ichikawa K, Node M, and Fujita E (1979) Hard acid and soft nucleophile system. New efficient method for removal of benzyl protecting group. *J. Org. Chem.* 44 (10), 1661–1664.
- (27). Lockner JW, Eubanks LM, Choi JL, Lively JM, Schlosburg JE, Collins KC, Globisch D, Rosenfeld-Gunn RJ, Wilson IA, and Janda KD (2015) Flagellin as carrier and adjuvant in cocaine vaccine development. *Mol. Pharmaceutics* 12 (2), 653–62.
- (28). Bode C, Zhao G, Steinhagen F, Kinjo T, and Klinman DM (2011) CpG DNA as a vaccine adjuvant. *Expert Rev. Vaccines* 10 (4), 499–511. [PubMed: 21506647]
- (29). Nelsen JL, Lapoint J, Hodgman MJ, and Aldous KM (2010) Seizure and coma following Kratom (*Mitragynina speciosa* Korth) exposure. *J. Med. Toxicol.* 6 (4), 424–6. [PubMed: 20411370]
- (30). Karinen R, Fosen JT, Rogde S, and Vindenes V (2014) An accidental poisoning with mitragynine. *Forensic Sci. Int.* 245, e29–32. [PubMed: 25453780]
- (31). McIntyre IM, Trochta A, Stolberg S, and Campman SC (2015) Mitragynine ‘Kratom’ related fatality: a case report with postmortem concentrations. *J. Anal. Toxicol.* 39 (2), 152–5. [PubMed: 25516573]



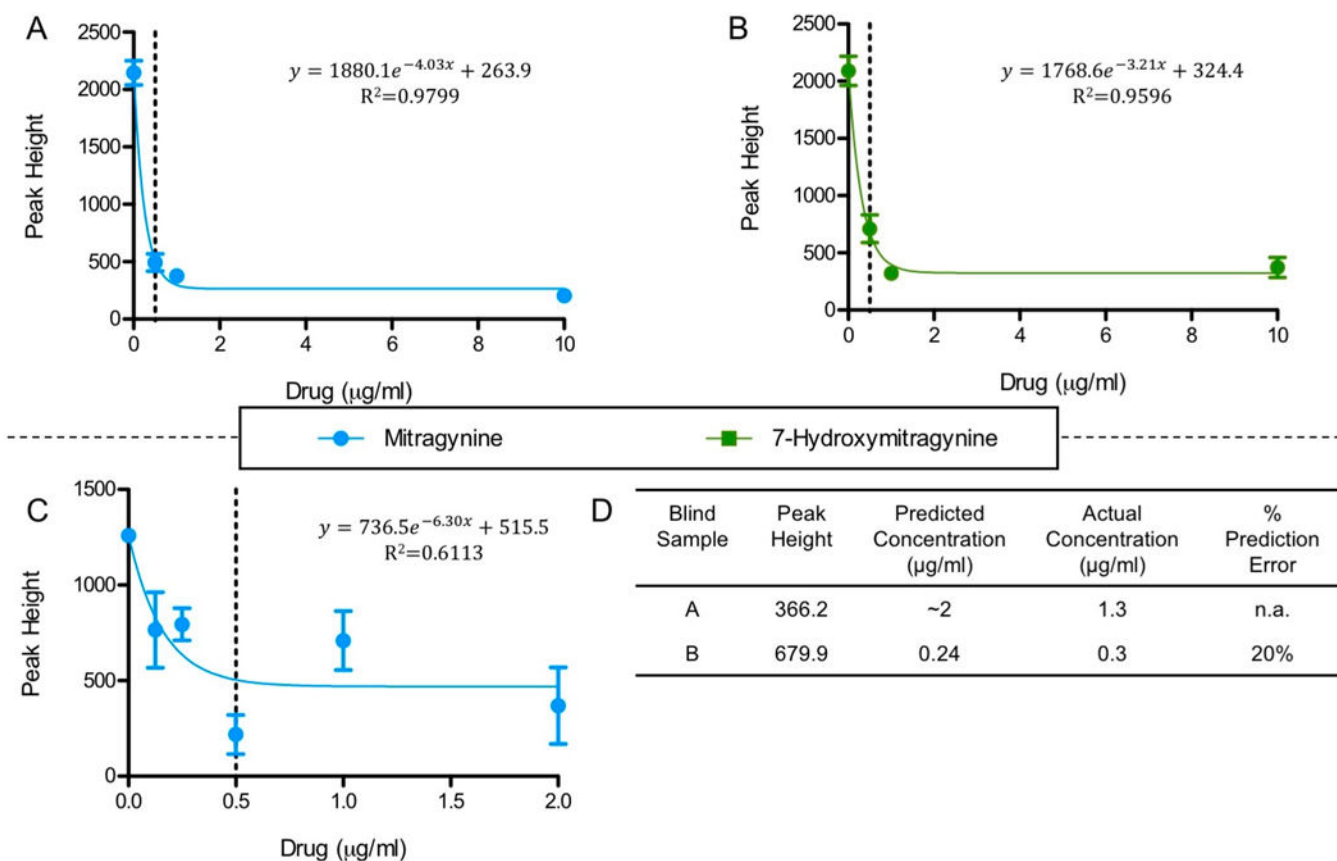
**Figure 1.** Kratom plant with its two main psychoactive alkaloids—mitragynine and 7-hydroxymitragynine—and their relative abundance in Kratom extract products.



**Figure 2.**

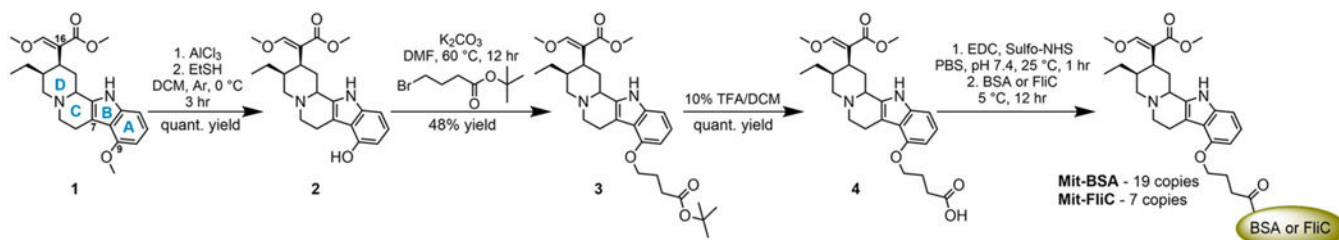
Summary of the three phases leading to the development of a lateral flow immunoassay for the detection of mitragynine, the major alkaloid found in kratom. (A) Hapten design and synthesis from commercially available mitragynine, immunoconjugation, and vaccine formulation with cytosine-phosphate-guanine oligonucleotide 1826 (CpG ODN 1826) and alum. The CpG ODN 1826 sequence and chemical formula of alum are both given. (B) Monoclonal antibody production in mice immunization with mitragynine vaccine, spleen harvest, B-cell isolation and sorting, and fusion with immortal myeloma cell line to produce monoclonal antibody hybridomas. (C) Lateral flow immunoassay strip design, production, and optimization; absorbent pad collects the runoff sample, test spot is loaded with Mit-BSA, conjugate pad is loaded with colloidal gold-conjugated antibody, and sample pad is applied with the liquid test sample. Negative tests, or samples with no drug, appear pigmented at the test spot as a result of the colloidal gold-conjugated antibody bound to the BSA conjugate without competition. Positive tests, or samples with high drug concentration, appear blank at the test spot as a result of the colloidal gold-conjugated antibody bound to drug instead of the BSA conjugate. BSA stands for bovine serum albumin, Mit-BSA stands for mitragynine conjugated to BSA. FliC is a bacterial flagellin protein used as a carrier protein due to its immunogenic potential.





**Figure 3.**

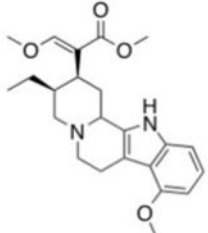
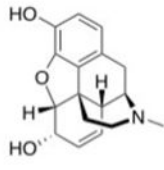
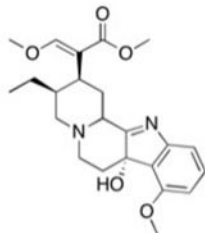

Standard curves for mitragynine in buffer (A), 7-hydroxymitragynine in buffer (B), and mitragynine in diluted urine (C), as peak height versus drug concentration. Equations displayed were fit to the data by one-phase exponential decay modeling. (D) Operator-blind mitragynine-spiked urine samples were measured and their concentrations were calculated using the mitragynine urine standard curve equation in panel C. Peak height is a background subtracted measurement of the visual intensity of the test spot, read on Leelu Benchtop Reader (Lumos Diagnostics). Percent prediction error is defined as  $\frac{\text{predicted Concentration} - \text{Actual Concentration}}{\text{Actual Concentration}} \times 100$  and was not calculated for sample A because the peak height was out of range for the standard curve equation.

**Scheme 1.**

Synthesis of Mitragynine Hapten, Mit-BSA and Mit-FliC Immunoconjugates

**Table 1.**

Lethality of Mitragynine and 7-Hydroxymitragynine Compared to Heroin

Relative $\mu$ -Opioid Receptor Potency <sup>a</sup>		
		
mitragynine	morphine	7-hydroxymitragynine
		
Lethality in Swiss Webster Males		
drug	LD <sub>50</sub>	
	iv	oral
mitragynine	27.8 (n.a.)	547.7 (477.1 <sup>c</sup> )
7-hydroxymitragynine	24.7 (n.a.)	n.d. <sup>d</sup>
heroin	23.7 (21.8 <sup>d</sup> )	n.a.

<sup>a</sup>On the basis of potency on the  $\mu$ -opioid receptors in the guinea pig ileum.<sup>11</sup><sup>b</sup>Literature value for LD<sub>50</sub> in mice<sup>c</sup>Literature value for LD<sub>50</sub> in Male Swiss albino mice.<sup>22</sup><sup>d</sup>No lethal outcomes were observed for mice when dosed orally in the range of 6.25–50 mg/kg.

**Table 2.**Vaccinated Mice Whole Sera IC<sub>50</sub> Values against Mitragynine and Midpoint Titers against Mit-BSA

mouse	IC <sub>50</sub> ( $\mu$ M) <sup>a</sup>	midpoint titers <sup>b</sup>	
		week 3	week 5
1	1.482	51200–102400	51200–102400
2	1.153	51200	51200
3	2.919	25600–51200	25600–51200
4	2.089	25600–51200	12800–25600

<sup>a</sup> Measured by surface plasmon resonance (SPR) against Mit-BSA with week 5 sera.<sup>b</sup> Measured by enzyme linked immunosorbent assay (ELISA) against Mit-BSA.

Author Manuscript

Author Manuscript

Author Manuscript

Author Manuscript

Table 3.

Midpoint Titers against Mit-BSA, IC<sub>50</sub> Values against Mitragynine Determined by SPR and Competitive ELISA, and Crude Lateral Flow Assay Scores for Select  $\alpha$ -Mitragynine mAbs<sup>a</sup>

mAb	midpoint titer	SPR <sup>b</sup>		competitive ELISA <sup>c</sup>		lateral assay score <sup>d</sup>	
		IC <sub>50</sub> ( $\mu$ M)	urine IC <sub>50</sub> ( $\mu$ g/mL)	urine IC <sub>50</sub> ( $\mu$ g/mL)	buffer IC <sub>50</sub> ( $\mu$ g/mL)	0 $\mu$ g/mL mitragynine	10 $\mu$ g/mL mitragynine
MIT11C2	1024–2048	0.1–1	0.037 ( $\pm$ 0.000)	0.446 ( $\pm$ 0.251)		4.5 ( $\pm$ 0.7)	0.5 ( $\pm$ 0.7)
MIT17B7	64–128	0.1–1	1.45 ( $\pm$ 0.000)	0.607 ( $\pm$ 0.321)		0.0 ( $\pm$ 0.0)	0.0 ( $\pm$ 0.0)
MIT29B7	128–256	0.1–1	3.28 ( $\pm$ 2.23)	1.23 ( $\pm$ 0.000)		9.0 ( $\pm$ 1.4)	4.0 ( $\pm$ 2.8)
MIT25G11	256+	1	0.912 ( $\pm$ 0.043)	0.098 ( $\pm$ 0.0004)		7.5 ( $\pm$ 3.5)	2.5 ( $\pm$ 2.1)
MIT17H11	256+	1–10	0.997 ( $\pm$ 0.000)	0.347 ( $\pm$ 0.028)		e	e

<sup>a</sup>Competitive ELISA was performed in buffer and urine as a predictor of lateral flow performance.

<sup>b</sup>SPR, measured against Mit-BSA.

<sup>c</sup>ELISA, measured against Mit-BSA plated with mitragynine (0.047–6  $\mu$ g/mL).

<sup>d</sup>Measured by eye with strongest “blank” sample being 10 and absence of color from gold nanoparticles being 0.

<sup>e</sup>mAb exhibit poor binding to gold nanoparticles, thus was unable to be tested for strip performance.

**Table 4.**

Binding Affinity of MIT11C2 and MIT29B7 to Mitragynine and 7-Hydroxymitragynine Determined by SPR

purified mAb	IC <sub>50</sub> (95% CI, nM)	
	mitragynine	7-OH mitragynine
MIT11C2	361.90 (61.43–2133)	557.10 (380.4–815.8)
MIT29B7	93.32 (49.70–175.2)	91.70 (65.87–127.7)

Author Manuscript

Author Manuscript

Author Manuscript

Author Manuscript